IEEE Access
Multidisciplinary ⋮ Rapid Review ⋮ Open Access Journal

Received January 2, 2021, accepted January 12, 2021, date of publication January 18, 2021, date of current version January 27, 2021.

Digital Object Identifier 10.1109/ACCESS.2021.3052085

An Improved Full-Order Sliding-Mode Observer for Rotor Position and Speed Estimation of SPMSM

WENJUN XU[1], SHAOCHENG QU[1], (Senior Member, IEEE), JINGHONG ZHAO[2], HONGRUI ZHANG[1], AND XIAONA DU[1]

[1]College of Physical Science and Technology, Central China Normal University, Wuhan 430079, China
[2]School of Electrical Engineering, Naval University of Engineering, Wuhan 430033, China

Corresponding author: Jinghong Zhao (zhaojinghong1213@163.com)

This work was supported in part by the National Natural Science Foundation of China under Grant 61673190/F030101, in part by the Self-Determined Research Funds of Central China Normal University (CCNU) from the Colleges Basic Research and Operation, Ministry of Education (MOE) under Grant CCNU18TS042, and in part by the Fundamental Research Funds for the Central Universities through the Innovation Funding Program under Grant 2020CXZZ103.

ABSTRACT This paper proposed an improved full-order sliding-mode observer (IFSMO), applied to a sensorless control system of surface-mounted permanent magnet synchronous motor (SPMSM), to obtain a high-precision rotor speed and position. First, the IFSMO method, which combines the new sliding-mode function with the variable boundary layer function, is presented to suppress the chattering and accelerate the convergence speed of the system. Meanwhile, since the observer has the characteristics of a second-order low-pass filter, the high-frequency noise contained in the estimated back EMF signal can be effectively filtered out without an additional low-pass filter. Then, the proposed PLL is designed to obtain rotor position and speed. Finally, simulations and experiments of the SPMSM system based on the IFSMO method under different working conditions are implemented, which demonstrates the effectiveness of the proposed algorithm.

INDEX TERMS Full-order sliding-mode observer (FSMO), rotor speed and position, surface-mounted permanent magnet synchronous motor (SPMSM), phase-locked loop (PLL).

I. INTRODUCTION

At present, there are three common drive methods used in PMSMs: variable voltage variable frequency control (VF) [1], [2], direct torque control (DTC) [3], and vector control [4], [5]. Among these three control methods, the VF control method cannot control torque, thus this method has poor speed control performance and low efficiency; the DTC method has high noise and large torque ripple. The vector control technology is used in most SPMSM control systems due to its small torque ripple and large speed range [6], [7].

On the other hand, the speed control methods of the sSPMSM system can be divided into two categories: the first is sensor control mode, which measures the rotor speed and position information by the mechanical sensor. The second is the sensorless control method, which uses algorithm instead of sensor to obtain rotor position and speed information [25]. Because the sensorless control technology omits sensors, it solves the problems existing in the installation of mechanical sensors, simplifies the structure of the control system, reduces the cost of the system, and has strong reliability [9]. Therefore, the sensorless control technology has been extensively applied in the high-performance speed control systems [10]–[12].

There are two kinds of sensorless control methods: the observer methods and the high-frequency (HF) signal injection method [13]. The observer methods take the voltage and current of the motor as the observer input, so as to observe the rotor position. And the observer methods include extended Kalman filter [15], the model reference adaptive [14], and sliding-mode observer (SMO) [16], etc. Among them, the extended Kalman filter method and model reference adaptive method depend upon the motor model, and the accuracy of the model will determine the estimation

The associate editor coordinating the review of this manuscript and approving it for publication was Jinquan Xu.

accuracy of the rotor position. For the HF method, it is applicable for low-speed motor operation, which requires high accuracy of signal detection. At the same time, the injection of high-frequency excitation is prone to generate high-frequency noise, which degrades system performance [17].

Compared with other methods, the SMO method has the merits of strong robustness to disturbance, low sensitivity to model parameter changes, and a simple algorithm, which can solve the influence of system parameter change and disturbance [11], [18]. However, conventional SMO uses arctangent to estimate the rotor position, which is complicated to calculate and has poor anti-disturbance ability [21]. In addition, in the sliding mode variable structure system, the switching function will appear time delay and space hysteresis due to the inertia, which will cause high-frequency components in the equivalent back EMF. Moreover, this phenomenon will lead to large errors of the rotor speed and information, which affects the performance of the SPMSM system [20].

To address these issues, kinds of research on sliding-mode control in the field of sensorless PMSM control have been carried out [23]. In [22], a second-order SMO is designed to observe the rotor position of a PMSM, but an additional low-pass filter (LPF) is required to filter out the sliding-mode noise. In order to avoid using a LPF, a state observer is added to observe the back EMF [19], and a full-order SMO is designed to observe the back EMF [23]. These two methods can achieve a good control effect in the middle and high-speed range. But with the decrease of rotor speed, the back EMF gradually decreases, and the accuracy of observation will also be reduced. To improve the accuracy of the rotor position and speed at low speed, an adaptive-gain SMO for sensorless PMSM system is presented [24]. However, this method still needs to design an additional LPF and compensate for the angle delay. To avoid the phase delay caused by the LPF, an adaptive super-twisting method based upon SMO for the PMSM drive system is introduced, which enhances the performance of the system at a low speed [8].

To suppress sliding-mode chattering and improve the response speed of the system, an IFSMO is proposed by combining the new sliding-mode function with an adaptive switching function. Due to the existence of the new sliding-mode function, the response speed of the system state is improved. And the boundary layer function effectively suppresses the sliding-mode chattering. Meanwhile, the back EMF observer has the attributes of the second-order LPF, which further reduces the high-frequency noise. By comparing the simulation results of the conventional FSMO method with those of the IFSMO algorithm, it is proved that the SPMSM system under the IFSMO method has the performance of high precision and strong robustness.

This paper is divided into six sections: section I is an introduction; section II introduces the mathematical model of SPMSM; section III compares the differences between the conventional FSMO and the proposed IFSMO; section IV gives simulation waveform and analysis; section V presents experimental results and analysis; section VI concludes this paper.

II. MATHEMATICAL MODEL

The mathematical model of SPMSM in a two-phase ($\alpha - \beta$) stationary coordinate system is expressed as [27]

$$\begin{cases} pL_s i_\alpha = -R_s i_\alpha + u_\alpha + e_\alpha \\ pL_s i_\beta = -R_s i_\beta + u_\beta + e_\beta \\ e_\alpha = \omega_e \lambda_f \sin\theta_e \\ e_\beta = -\omega_e \lambda_f \cos\theta_e \end{cases} \tag{1}$$

where u_α, u_β u_α, u_β, i_α, i_β and e_α, e_β are the phase voltage, stator current, and back EMF voltage in the $\alpha - \beta$ axis, respectively. ω_e is the electrical angular speed, λ_f is the flux linkage, θ_e is the rotor electrical position. And R_s is the winding resistance, L_s is the winding inductance, and p represents a differential operator.

Since the rate change of stator current is much greater than the rate of change of the electric angular speed during a sampling period, suppose $\dot{\omega}_e \approx 0$. Hence, the relationship between the back EMF and its change rate satisfies the following formula

$$\begin{cases} pe_\alpha = -\omega_e e_\beta \\ pe_\beta = \omega_e e_\alpha \end{cases} \tag{2}$$

According to (2), (1) can be further expressed as

$$\begin{cases} pi_\alpha = -\dfrac{R_s}{L_s} i_\alpha + \dfrac{1}{L_s} u_\alpha + \dfrac{1}{L_s} e_\alpha \\ pi_\beta = -\dfrac{R_s}{L_s} i_\beta + \dfrac{1}{L_s} u_\beta + \dfrac{1}{L_s} e_\beta \\ pe_\alpha = -\omega_e e_\beta \\ pe_\beta = \omega_e e_\alpha \end{cases} \tag{3}$$

III. THE PROPOSED IFSMO

A. THE DESIGN OF IFSMO

Combining (1) and (2), the full-order state equation of SPMSM with stator current and back EMF as state variables is obtained

$$\frac{d}{dt}\begin{bmatrix} \mathbf{i_s} \\ \mathbf{e_s} \end{bmatrix} = \begin{bmatrix} A & B \\ 0 & C \end{bmatrix}\begin{bmatrix} \mathbf{i_s} \\ \mathbf{e_s} \end{bmatrix} + \begin{bmatrix} D \\ 0 \end{bmatrix}\mathbf{u_s} \tag{4}$$

where $\mathbf{i_s} = [i_\alpha, i_\beta]^T$, $\mathbf{e_s} = [e_\alpha, e_\beta]^T$, $\mathbf{u_s} = [u_\alpha, u_\beta]^T$, $A = -\frac{R_s}{L_s}\Lambda$, $B = -\frac{1}{L_s}\Lambda$, $C = \omega_e I$, $D = -B\Lambda = \begin{bmatrix} 1 & 0 \\ 0 & 1 \end{bmatrix}$, $I = \begin{bmatrix} 0 & -1 \\ 1 & 0 \end{bmatrix}$.

According to (4), the IFSMO equation is expressed as

$$\frac{d}{dt}\begin{bmatrix} \hat{\mathbf{i}}_\mathbf{s} \\ \hat{\mathbf{e}}_\mathbf{s} \end{bmatrix} = \begin{bmatrix} A & B \\ 0 & \hat{C} \end{bmatrix}\begin{bmatrix} \hat{\mathbf{i}}_\mathbf{s} \\ \hat{\mathbf{e}}_\mathbf{s} \end{bmatrix} + \begin{bmatrix} D \\ 0 \end{bmatrix}\mathbf{u_s} - E\mathbf{\Gamma_s} \tag{5}$$

where $\hat{\mathbf{i}}_\mathbf{s} = [\hat{i}_\alpha, \hat{i}_\beta]^T$, $\mathbf{e_s} = [\hat{e}_\alpha, \hat{e}_\beta]^T$, $\mathbf{\Gamma_s} = [\Gamma_\alpha, \Gamma_\beta]^T$, $\hat{C} = \hat{\omega}_e I$ and $E = \frac{1}{L_s}\begin{bmatrix} k & 0 & -m & 0 \\ 0 & k & 0 & -m \end{bmatrix}^T$, E is the feedback gain

matrix; k and m represent the switching gains of the IFSMO; and

$$\mathbf{\Gamma_s} = \begin{cases} \text{sgn}(\mathbf{s}) & if\ |\mathbf{s}| \geq \Delta \\ H(\mathbf{s}) & if\ |\mathbf{s}| < \Delta \end{cases} \tag{6}$$

$H(\mathbf{s}) = 1 - \frac{2}{e^{2\delta \mathbf{s}}+1}$, $\delta = \pi/\Delta$, Δ is the boundary layer thickness.

Remark 1: Compared with the traditional switching function, the switching function in this paper is a variable boundary layer function, which has fast convergence speed and small chattering due to the existence of δ.

Moreover, in order to speed up the convergence rate of system states, a novel integral sliding-mode function is designed as

$$\mathbf{s} = \begin{bmatrix} s_\alpha \\ s_\beta \end{bmatrix} \triangleq \begin{bmatrix} \tilde{i}_\alpha + \chi \text{sgn}^\gamma(\tilde{i}_\alpha) \\ \tilde{i}_\beta + \chi \text{sgn}^\gamma(\tilde{i}_\beta) \end{bmatrix} \tag{7}$$

where χ and γ are constants with $\chi \in (0, R_s/L_s)$.

Remark 2: The designed sliding-mode function consists of continuous term and discontinuous term, in which the continuous term can promote the system state to maintain a good continuity during the switching process, and the discontinuous term can make the system state maintain fast convergence in the sliding-mode reaching process.

Subtracting (5) from (4), the state equations of current error and back EMF error are obtained as follows

$$\frac{d}{dt}\begin{bmatrix} \tilde{\mathbf{i}}_\mathbf{s} \\ \tilde{\mathbf{e}}_\mathbf{s} \end{bmatrix} = \begin{bmatrix} A & B \\ 0 & C \end{bmatrix}\begin{bmatrix} \tilde{\mathbf{i}}_\mathbf{s} \\ \tilde{\mathbf{e}}_\mathbf{s} \end{bmatrix} + \tilde{C}\begin{bmatrix} \mathbf{0} \\ \hat{\mathbf{e}}_\mathbf{s} \end{bmatrix} - E\begin{bmatrix} \Gamma_\alpha \\ \Gamma_\beta \end{bmatrix} \tag{8}$$

where $\tilde{\mathbf{i}}_\mathbf{s} = [\tilde{i}_\alpha, \tilde{i}_\beta]^T$, $\tilde{\mathbf{e}}_\mathbf{s} = [\tilde{e}_\alpha, \tilde{e}_\beta]^T$, $\tilde{C} = \tilde{\omega}_e I$, $\tilde{\omega}_e$ is the error speed of the rotor.

B. STABILITY ANALYSIS OF IFSMO

Firstly, the stability of the sliding-mode current observer is analyzed. The Lyapunov function is constructed as follows [26]

$$V_1 = \frac{1}{2}\mathbf{s}^T\mathbf{s} \tag{9}$$

When $\dot{V}_1 < 0$ is satisfied, the reachability and existence conditions of sliding-mode are satisfied.

Differentiating (9) obtains

$$\dot{V}_1 = \mathbf{s}^T\dot{\mathbf{s}} = s_\alpha(\dot{\tilde{i}}_\alpha + \chi\gamma|\tilde{i}_\alpha|^{\gamma-1}\dot{\tilde{i}}_\alpha) + s_\beta(\dot{\tilde{i}}_\beta + \chi\gamma|\tilde{i}_\beta|^{\gamma-1}\dot{\tilde{i}}_\beta) \tag{10}$$

Define

$$\begin{cases} \dot{\Theta}_\alpha = s_\alpha(\dot{\tilde{i}}_\alpha + \chi\gamma|\tilde{i}_\alpha|^{\gamma-1}\dot{\tilde{i}}_\alpha) \\ \dot{\Theta}_\beta = s_\beta(\dot{\tilde{i}}_\beta + \chi\gamma|\tilde{i}_\beta|^{\gamma-1}\dot{\tilde{i}}_\beta) \end{cases} \tag{11}$$

then, (10) can be rewritten $\dot{V}_1 = \dot{\Theta}_\alpha + \dot{\Theta}_\beta$.

According to (7), (8), $\dot{\Theta}_\alpha$ yields

$$\begin{aligned} \dot{\Theta}_\alpha &= s_\alpha(\dot{\tilde{i}}_\alpha + \chi\gamma|\tilde{i}_\alpha|^{\gamma-1}\dot{\tilde{i}}_\alpha) = (1+\chi\gamma|\tilde{i}_\alpha|^{\gamma-1})s_\alpha\dot{\tilde{i}}_\alpha \\ &= \frac{1}{L_s}(-R_s\tilde{i}_\alpha - \tilde{e}_\alpha - k\Gamma_\alpha)(1+\chi\gamma|\tilde{i}_\alpha|^{\gamma-1})s_\alpha \\ &= (-\frac{R_s\tilde{i}_\alpha}{L_s}(\tilde{i}_\alpha + \chi|\tilde{i}_\alpha|^\gamma \text{sgn}(\tilde{i}_\alpha)) - \frac{s_\alpha(\tilde{e}_\alpha + k\Gamma_\alpha)}{L_s}) \\ &\quad \times (1+\chi\gamma|\tilde{i}_\alpha|^{\gamma-1}) \\ &= (-\frac{R_s}{L_s}(\tilde{i}_\alpha^2 + \chi|\tilde{i}_\alpha|^{\gamma+1}) - \frac{s_\alpha}{L_s}(\tilde{e}_\alpha + k\Gamma_\alpha)) \\ &\quad \times (1+\chi\gamma|\tilde{i}_\alpha|^{\gamma-1}) \end{aligned} \tag{12}$$

Additionally,

$$-\frac{R_s}{L_s}(\tilde{i}_\alpha^2 + \chi|\tilde{i}_\alpha|^{\gamma+1}) \leq 0 \tag{13}$$

$$1 + \chi\gamma|\tilde{i}_\alpha|^{\gamma-1} > 0 \tag{14}$$

Hence, when $k > |\frac{\tilde{e}_\alpha}{\Gamma_\alpha}|$ is satisfied, $\dot{\Theta}_\alpha \leq 0$. Similarly, when $k > |\frac{\tilde{e}_\beta}{\Gamma_\beta}|$, we obtain

$$\begin{aligned} \dot{V}_\beta &= (-\frac{R_s}{L_s}(\tilde{i}_\beta^2 + \chi|\tilde{i}_\beta|^{\gamma+1}) - \frac{s_\beta}{L_s}(\tilde{e}_\beta + k\Gamma_\beta))(1+\chi\gamma|\tilde{i}_\beta|^{\gamma-1}) \\ &\leq 0 \end{aligned} \tag{15}$$

Hence, when

$$k > \max\{|\frac{\tilde{e}_\alpha}{\Gamma_\alpha}|, |\frac{\tilde{e}_\beta}{\Gamma_\beta}|\} \tag{16}$$

We have

$$\dot{V}_1 = \dot{\Theta}_\alpha + \dot{\Theta}_\beta \leq 0 \tag{17}$$

Remark 3: The sliding-mode gain k, which just needs to be greater than the error value of the back EMF instead of its estimated value $k > \max(|\hat{e}_\alpha|, |\hat{e}_\beta|)$ in [20], can ensure the reachability condition of SMO. This is different from conventional SMO. The advantage of this design is that under the same convergence rate, the chattering of the system is smaller.

From (16) and (17), when the gain coefficient is between $-k_{\max}$ the $k_{\max}$, the sliding-mode current observer can satisfy the existence condition of the sliding-mode.

When the system state reaches the sliding-mode surface $\mathbf{i}_s = \dot{\mathbf{i}}_s = 0$, we can obtain

$$\begin{cases} \tilde{e}_\alpha = -k\Gamma_\alpha \\ \tilde{e}_\beta = -k\Gamma_\beta \end{cases} \tag{18}$$

According to (8) and (18), we can get

$$\begin{cases} \dot{\tilde{e}}_\alpha = -(\hat{\omega}_e - \omega_e)\hat{e}_\beta - \omega_e\tilde{e}_\beta + M\Gamma_\alpha \\ \dot{\tilde{e}}_\beta = (\hat{\omega}_e - \omega_e)\hat{e}_\alpha + \omega_e\tilde{e}_\alpha + M\Gamma_\beta \end{cases} \tag{19}$$

where $M = m/(kL_s)$.

Then a Lyapunov function of the back EMF is defined as

$$V_2 = \frac{1}{2}(\tilde{e}_\alpha^2 + \tilde{e}_\beta^2) \tag{20}$$

The time derivative of (20) yields

$$\begin{aligned} \dot{V}_2 &= \dot{\tilde{e}}_\alpha\tilde{e}_\alpha + \dot{\tilde{e}}_\beta\tilde{e}_\beta \\ &= (-\tilde{\omega}_e\hat{e}_\beta - \omega_e\tilde{e}_\beta - M\tilde{e}_\alpha)\tilde{e}_\alpha + (\tilde{\omega}_e\hat{e}_\alpha + \omega_e\tilde{e}_\alpha - M\tilde{e}_\beta)\tilde{e}_\beta \\ &= -M(\tilde{e}_\alpha^2 + \tilde{e}_\beta^2) + \tilde{\omega}_e(\hat{e}_\alpha\tilde{e}_\beta - \tilde{e}_\alpha\hat{e}_\beta) \end{aligned} \tag{21}$$

To guarantee the stability of the back EMF observer and the existence of the sliding-mode surface, it is necessary to satisfy $\dot{V}_2 < 0$, which yields

$$M > \max\{\frac{\tilde{\omega}_e(\hat{e}_\alpha\tilde{e}_\beta - \tilde{e}_\alpha\hat{e}_\beta)}{\tilde{e}_\alpha^2 + \tilde{e}_\beta^2}\} \tag{22}$$

C. CHATTERING SUPPRESSION ANALYSIS

According to (4), we can obtain

$$\begin{cases} \dot{\hat{e}}_\alpha = -\hat{\omega}_e\hat{e}_\beta + M\Gamma_\alpha \\ \dot{\hat{e}}_\beta = \hat{\omega}_e\hat{e}_\alpha + M\Gamma_\beta \end{cases} \tag{23}$$

From (23), the back EMF can be expressed as follows

$$\begin{cases} \hat{e}_\alpha = \dfrac{M}{s^2 + \hat{\omega}_e^2}(s\Gamma_\alpha - \hat{\omega}_e\Gamma_\beta) \\ \hat{e}_\beta = \dfrac{M}{s^2 + \hat{\omega}_e^2}(s\Gamma_\beta + \hat{\omega}_e\Gamma_\alpha) \end{cases} \tag{24}$$

where s is the Laplace operator.

Remark 4: According to (24), although the term $s\Gamma_\alpha - \hat{\omega}_e\Gamma_\beta$ contains high-frequency noise in the back EMF signal, the noise is well filtered out because $M/(s^2 + \hat{\omega}_e^2)$ behaves as a second-order LPF. Besides, due to the existence of the second-order LPF, both the design of the LPF and angle compensation are not required, which simplifies the system algorithm.

D. THE PROPOSED PLL

To obtain precise rotor position and speed, a normalized phase-locked loop (PLL) is introduced to suppress the variations of system bandwidth due to the change of back EMF. Meanwhile, a signal suppressor is designed to attenuate the step signal during the convergence of Δe, which effectively improves the accuracy of the rotor position signal. The improved PLL structure diagram is shown in Fig. 1. The PLL consists of a phase detector (PD), a loop filter (LF), and a voltage-controlled oscillator (VCO). After adjusting the angle error $\Delta\theta_e$ through the proportional integration link and the signal suppressor, the rotor speed is obtained. Then the rotor speed goes through a differential link to obtain the rotor position.

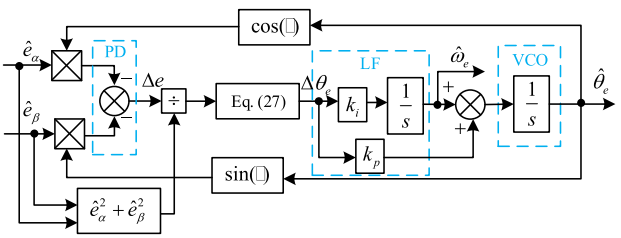

FIGURE 1. Structure diagram of the proposed PLL.

From Fig. 1, we can get

$$\begin{aligned} \Delta e &= -\hat{e}_\alpha\cos\hat{\theta}_e - \hat{e}_\beta\sin\hat{\theta}_e \\ &= E\sin(\theta_e - \hat{\theta}_e) \end{aligned} \tag{25}$$

where $E = \psi_f\omega_e$ and its amplitude mainly depends on the rotational speed.

Remark 5: Usually when $|\theta_e - \hat{\theta}_e| < \frac{\pi}{6}$, it can be assumed that $\sin(\theta_e - \hat{\theta}_e) \approx \theta_e - \hat{\theta}_e$. However, in the case of local linear approximation, the third-order term is omitted from the error formula of the conventional PLL system, resulting in large errors in the dynamic response of the system. The Taylor formula of error term $\sin(\theta_e - \hat{\theta}_e) \approx (\theta_e - \hat{\theta}_e)$ can be expanded as

$$\sin(\theta_e - \hat{\theta}_e) = (\theta_e - \hat{\theta}_e) + \frac{(\theta_e - \hat{\theta}_e)^3}{3} \tag{26}$$

For better suppression and to ensure the stability of the PLL system, (25) can be redesigned as

$$\Delta\theta_e = E((\theta_e - \hat{\theta}_e) + (\theta_e - \hat{\theta}_e)^3/3) \tag{27}$$

As shown in Fig. 1, the differential equation of the rotor speed and position is formulated as follows

$$\frac{d}{dt}\begin{bmatrix} \hat{\omega}_e \\ \hat{\theta}_e \end{bmatrix} = \begin{bmatrix} 0 & 0 \\ 1 & 0 \end{bmatrix}\begin{bmatrix} \hat{\omega}_e \\ \hat{\theta}_e \end{bmatrix} + \Delta\theta_e\begin{bmatrix} k_i \\ k_p \end{bmatrix} \tag{28}$$

where k_i and k_p are integral gain and proportional gain respectively.

The characteristic polynomial of the equation (28) is $s^2 + k_p s + k_i$. If the gains k_p and k_i are properly selected, the poles of the estimator (28) can be located at any position. To enhance the robustness of the observer (28) and avoid system oscillations, the poles should be located at $s = -\lambda$, where λ is a normal number. Accordingly, the characteristic polynomial is $s^2 + 2\lambda s + \lambda^2$, so the gain can be designed as

$$\begin{cases} k_i = \dfrac{\lambda^2}{E} \\ k_p = \dfrac{2\lambda}{E} \end{cases} \tag{29}$$

In order to further optimize the gain (29) of the observer, λ must be reduced correspondingly when the speed is reduced to the set critical speed. Here we design $\lambda = |\omega_e|\lambda_0/\omega_e^\Delta$, where ω_e^Δ is the set critical speed and λ_0 is the corresponding value at a different speed. Then the gain can be expressed as follows

$$k_i = \begin{cases} \dfrac{\lambda_0^2}{\hat{\omega}_e\psi_f} & if\ |\omega_e| \geq \omega_e^\Delta \\ \dfrac{\lambda_0^2\hat{\omega}_e}{(\omega_e^\Delta)^2\psi_f} & if\ |\omega_e| < \omega_e^\Delta \end{cases} \tag{30}$$

$$k_p = \begin{cases} \dfrac{2\lambda_0}{\hat{\omega}_e\psi_f} & if\ |\omega_e| \geq \omega_e^\Delta \\ \dfrac{2\lambda_0 H(\omega_e)\omega_e}{\omega_e^\Delta\psi_f} & if\ |\omega_e| < \omega_e^\Delta \end{cases} \tag{31}$$

Remark 6: During actual motor operation, external perturbations may make the rotor speed too large or too small, and the gain of the observer is inversely proportional to the estimated speed. Different from the fixed PI method, the adaptive method in (30) and (31) can dynamically adjust the parameters λ_0 to keep the system in an optimal state, so as to reduce the impact of external disturbances on the system.

E. CLOSED-LOOP STABILITY ANALYSIS

According to the above analysis, the stability of IFSMO can be guaranteed. In addition, the PLL system is also stable because the poles of the system function are all located in the left half-plane. In order to further ensure the closed-loop stability of the system, a reconstruction technique is used to feed the estimated speed to a PI feedback controller. The PI control law of the rotor speed is designed as [27]

$$\Phi = K_1 x_1 + K_2 x_2 \tag{32}$$

$$\begin{cases} x_1 = \omega_e^* - \hat{\omega}_e \\ x_2 = \int_0^t x_1 d\tau = \int_0^t (\omega_e^* - \hat{\omega}_e) d\tau \end{cases} \tag{33}$$

where K_1, K_2 are positive constants, and ω_e^* is the reference electrical angular velocity of the motor.

Remark 7: By tuning the PI values of K_1, K_2 reasonably, the speed error x_1 can be maintained at a minimum. When the given speed ω_e^* is too large or the disturbance is too strong, the control law Φ will approach the saturation state to maintain the normal operation of the system. Therefore, the stability of the closed-loop system is guaranteed to a certain extent.

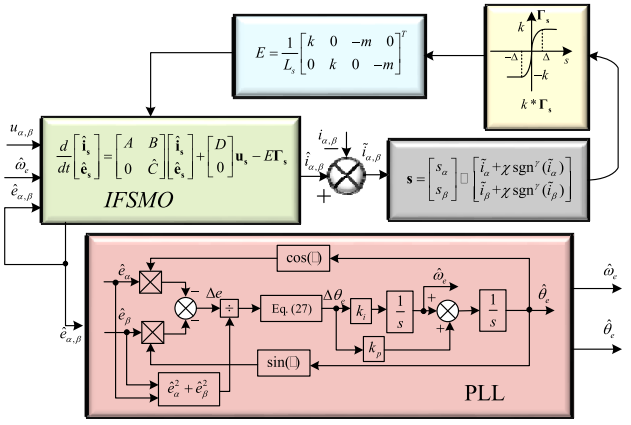

FIGURE 2. Structural diagram of IFSMO combined with PLL.

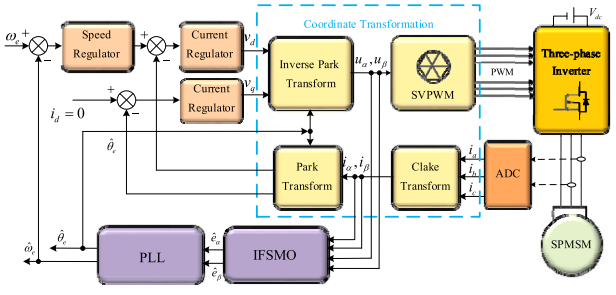

FIGURE 3. Structure of the proposed sensorless SPMSM system.

IV. SIMULATION ANALYSIS

In this section, MATLAB/Simulink is used to test the sensorless SPMSM system based on IFSMO and FSMO methods, respectively. The structural diagram of the IFSMO method combined with PLL is shown in Fig. 2. As is shown in Fig. 3, the structure of the proposed sensorless SPMSM system based on the IFSMO method is constructed by using $i_d = 0$ the current control mode. The main parameters of SPMSM are shown in Table 1 below. And the main parameters of the sensorless control system under the two methods are shown in Table 2.

TABLE 1. Main SPMSM parameters.

Parameters		Values
Stator resistance	R_s	205mΩ
Stator inductance	L_s	0.1mH
Flux linkage	λ_f	0.25 Wb
Rated Voltage	V_{dc}	30 V
Moment inertia	J	$0.0015\ kg \cdot m^2$
Pole pair	P_n	4

TABLE 2. Parameters under the two methods.

Methods	Values
FSMO	$k = 200, m = 125$ Current PI controller: $k_{pc} = 0.3,\ k_{ic} = 400$ Speed PI controller: $k_{ps} = 0.5,\ k_{is} = 0.02$
IFSMO	$k = 200, m = 125, \chi = 2, \gamma = 3/5, and\ M = 300$, $\omega_e^{\Delta} = 10$ Current PI controller: $k_{pc} = 0.3,\ k_{ic} = 400$ Speed PI controller: $k_{ps} = 0.5,\ k_{is} = 0.02$

A. SIMULATIONS UNDER CONVENTIONAL FSMO

Fig. 4 shows the simulation waveforms of the SPMSM system under the conventional FSMO, where the rotor steps from 0 r/min to a given rotational speed of 1000 r/min. Fig. 4(a) displays the simulation results of the rotor rising from a stationary state to 1000 r/min, and the response time of the rotor speed is about 10ms. It can be seen from Fig. 4(b) that when the rotor reaches the steady-state, the rotor speed fluctuates at 15 r/min. Fig. 4(c) shows the estimated back EMF waveform and Fig. 4(d) depicts the Lissajous curve of the estimated back EMF. It can be observed from Figs. 4(c) and (d) that high-frequency noises exist in the back EMF signal, which may affect the accuracy of rotor position and speed. Fig. 4(e) shows the actual rotor position and the estimated rotor position. From Fig. 4(e), it can be noticed that the estimated rotor position lags behind the actual rotor position. Fig. 4(f) depicts the estimated error of the rotor position, which is approximately 0.05 rad.

Fig. 5 represents the simulation waveforms of the rotor from 0 to 100 r/min under the conventional FSMO. Fig. 5(a) shows the dynamic response of the rotor speed, where it takes 13 ms for the rotor speed to go from standstill to 100 r/min. And as shown in Fig. 5(b), when the rotor

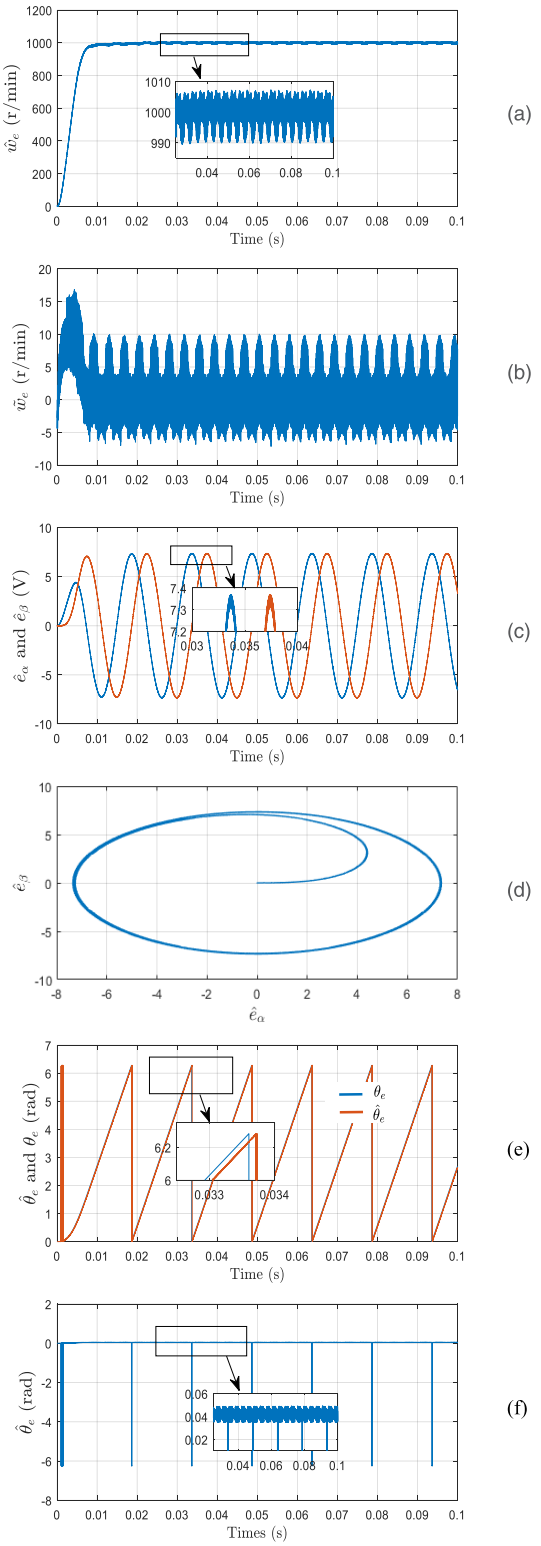

FIGURE 4. Simulation waveforms of the rotor running at 1000 r/min when using the conventional FSMO. (a) Estimated speed. (b) Speed error. (c) Estimated back EMF signals. (d) Lissajous curve of back EMF. (e) Actual position and estimated position. (f) Position error.

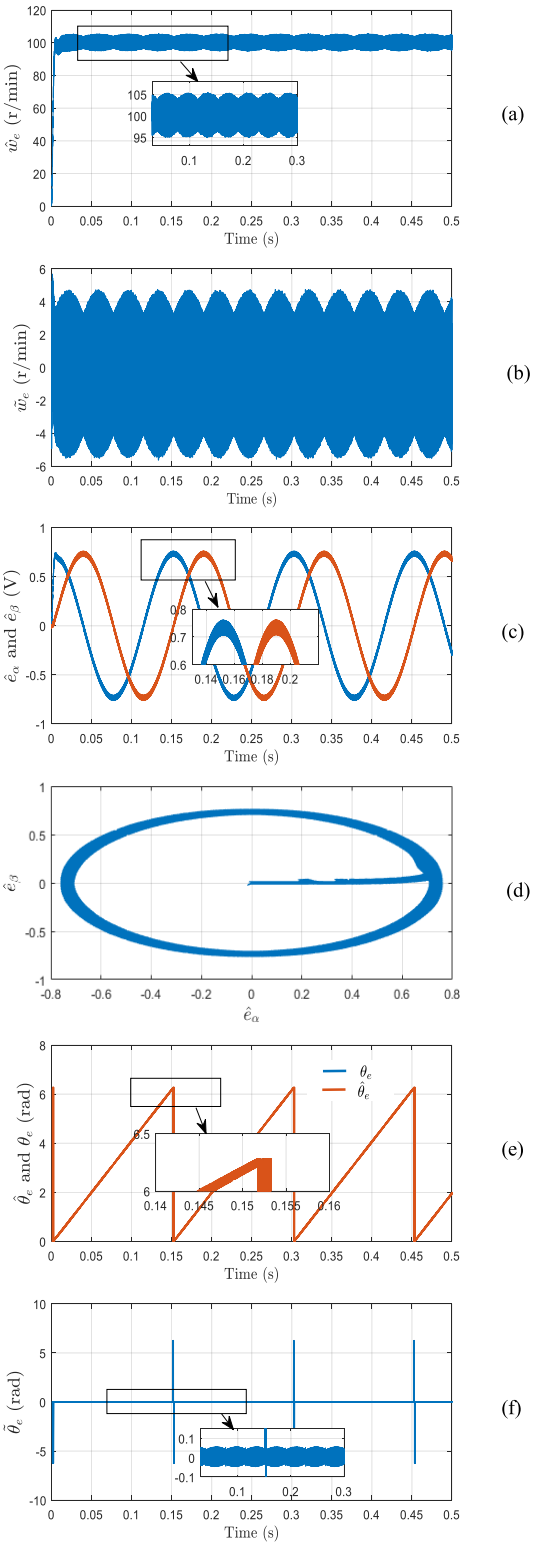

FIGURE 5. Simulation waveforms of the rotor running at 100 r/min when using the conventional FSMO. (a) Estimated speed. (b) Speed error. (c) Estimated back EMF signals. (d) Lissajous curve of back EMF. (e) Actual position and estimated position. (f) Position error.

reaches the steady-state, the fluctuation range of rotor speed is 9.5 r/min. Fig. 5(c) shows the estimated back EMF waveform of the rotor and Fig. 5(d) depicts the Lissajous curve of the estimated back EMF. It is observed that as the speed decreases, the amplitude of the back EMF becomes smaller. Fig. 5(e) shows the actual rotor position and the estimated

rotor position. From Fig. 5(e), it is noticed that the estimated rotor position lags behind the actual rotor position. Fig. 5(f) shows that the estimated error of the rotor position is about 0.1 rad.

B. SIMULATIONS UNDER CONVENTIONAL FSMO

Fig. 6 shows the simulation waveforms of the rotor under the IFSMO method, where the rotor changes from a stationary state to a given rotational speed of 1000 r/min. Fig. 6(a) represents the response process of the rotor speed, which rises from a standstill to 1000 r/min. From Fig. 6(a), the response time of rotor speed is 5 ms. And as illustrated in Fig. 6(b), when the rotor reaches the steady-state, the fluctuation range of rotor speed is 0.3 r/min. Moreover, the maximum speed error is only 2 r/min in the starting process. Fig. 6(c) shows the back EMF signal of the rotor in rotational coordinates and Fig. 6(d) illustrates the Lissajous curve of the estimated back EMF. Fig. 6(e) shows the actual rotor position and the estimated rotor position. From Fig. 6(e), it can be noticed that the estimated rotor position almost coincides with the actual rotor position, and the error of the rotor position is approximately zero as shown in Fig. 6(f).

Fig. 7 represents the simulation waveforms of the rotor from 0 r to 100 r/min under the IFSMO method. Fig. 7(a) shows the speed response waveform, where the rotor takes 7 ms from standstill to 100 r/min. From Fig. 7(b), when the rotor reaches the steady-state, the rotor speed fluctuates at 0.15 r/min. And the maximum speed error of the rotor is 0.55 r/min in the start-up process. Fig. 7(c) represents the estimated back EMF waveform and Fig. 7(d) represents the Lissajous curve of the estimated back EMF. Fig. 7(e) depicts the actual rotor position and the estimated rotor position. From Fig. 7(e), it can be noticed that the actual rotor position is almost consistent with the estimated rotor position. Fig. 7(f) shows the estimated error of the rotor position, which is almost zero.

C. COMPARATIVE ANALYSIS OF TWO METHODS

Figs. 4 and 6 show the results of the motor running at 1000 r/min under the FSMO and IFSMO methods, respectively. Comparing the results of Fig. 4(a)-(b) and Fig. 6(a)-(b), the response speed of the SPMSM system under the IFSMO method is faster than that of FSMO, and the steady-state error is smaller. According to the results in Figs. 4 (c) and (d) and Figs. 6 (c) and (d), compared with the back EMF obtained by the FSMO scheme, the back EMF estimated obtained by the IFSMO scheme is smoother and has less chattering. Besides, the estimated rotor position under the IFSMO method is consistent with the actual position without delay, but the rotor position using the FSMO method has a large error.

Figs. 5 and 7 show the results of the motor running at 100 r/min under the FSMO and IFSMO approaches, respectively. Comparing the simulation results in Figs 5 and 7, the waveforms of the back EMF signals and Lissajous curve are smooth under the IFSMO method. And the error value between actual and estimated rotor position is close to zero,

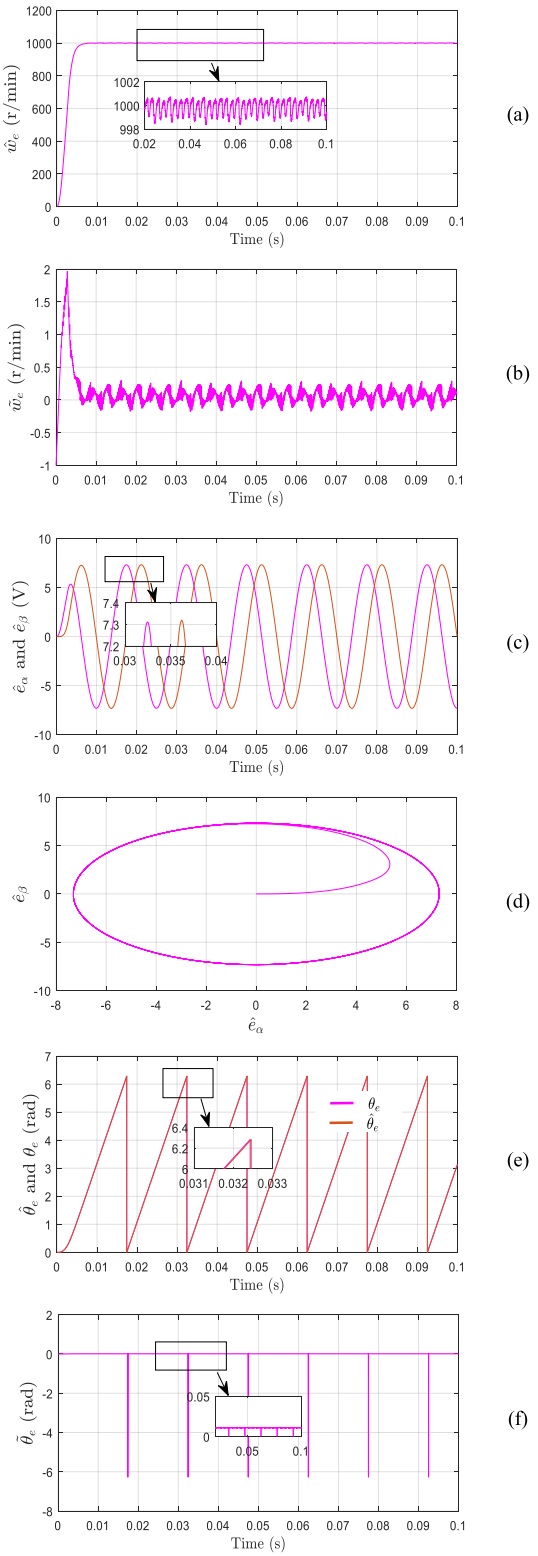

FIGURE 6. Simulation waveforms of the rotor running at 1000 r/min when using the IFSMO. (a) Estimated speed. (b) Speed error. (c) Estimated back EMF signals. (d) Lissajous curve of back EMF. (e) Actual position and estimated position. (f) Position error.

which indicates that the estimated rotor speed can accurately track the actual speed. Moreover, the motor can quickly converge to the given speed without overshoot during the start-up

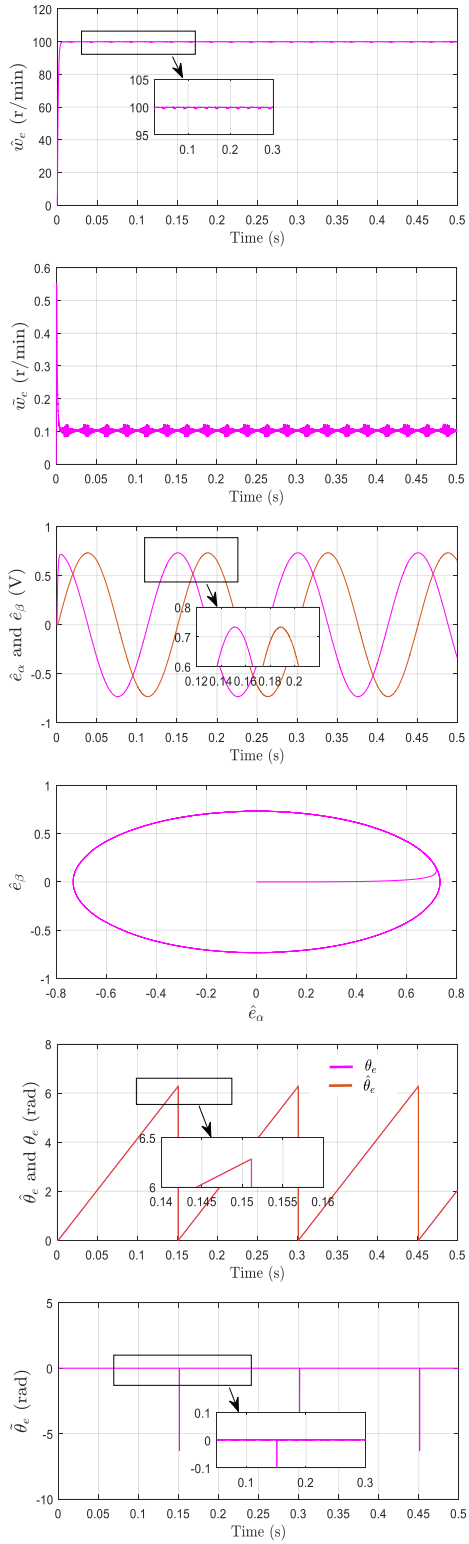

FIGURE 7. Simulation waveforms of the rotor running at 100 r/min when using the IFSMO. (a) Estimated speed. (b) Speed error. (c) Estimated back EMF signals. (d) Lissajous curve of back EMF. (e) Actual position and estimated position. (f) Position error.

process. And while the rotor is running steadily at 100 r/min under the IFSMO method, the steady-state speed error of the rotor will decrease from 9.5 to 0.15 r/min. It is obvious that the performance of the IFSMO is much better than that of the conventional FSMO. The performance indexes of the SPMSM system under the two methods are compared, as shown in Table 3.

TABLE 3. Comparison performances between IFSMO and FSMO.

Rotor speed	Index	FSMO	IFSMO
100 r/min	Convergence time	13 ms	7 ms
	speed steady-state fluctuation	9.5 r/min	0.15 r/min
	Maximum speed error	6 r/min	0.55 r/min
	Steady-state angle error	0.1 rad	0 rad
1000 r/min	Convergence time	10 ms	5 ms
	speed steady-state fluctuation	15 r/min	0.15 r/min
	Maximum speed error	15 r/min	2 r/min
	Steady-state angle error	0.05 rad	0 rad

According to the performance indexes listed in Table 3, compared with the conventional FSMO method, the IFSMO method has better characteristics in the sensorless SPMSM system, such as higher accuracy of rotor position and speed, and smaller system chattering. Moreover, the system under the IFSMO method has a fast convergence speed, little noise in steady-state, and good stability.

D. VARIOUS SPEEDS AND ROBUSTNESS ANALYSIS OF TWO METHODS

Fig. 8 shows the various speed profiles and the robustness of the SPMSM system under the IFSMO and FSMO methods, respectively. Fig. 8(a) indicates the variation of the rotor at different given speeds under the FSMO method. Fig. 8(b) indicates the variation of the rotor in various speed profiles under the IFSMO scheme. From Fig. 8(a), it can be seen that in the SPMSM system under the FSMO method, the rotor cannot reach an optimal state at different given speeds, and the speed error is large. However, after applying the IFSMO method under the same conditions, the rotor can track the given speed accurately with a small speed error. Figs. 8(c) and (d) show the simulation results under the FSMO and IFSMO methods when the rotor runs stably at 1000 r/min, then load $2N \cdot m$ is suddenly added to the system at 0.05s. From the comparison between Fig. 8(c) and Fig. 8(d), the speed fluctuation under the IFSMO method is smaller than that of the FSMO method. Meanwhile, the time for the rotor speed to reach a steady-state is shorter under the IFSMO method than that of the FSMO method.

V. EXPERIMENTAL ANALYSIS

The experimental platform includes a power supply, SPMSM control system, and load, in which the control unit is based on a PAC5223 chip. The controller has extensive hardware resources, such as a multi-channel PWM driver with dead time, three-phase current sampling, hardware over-current protection, management of voltage power supply, and a core capable of performing complex mathematical operations. The

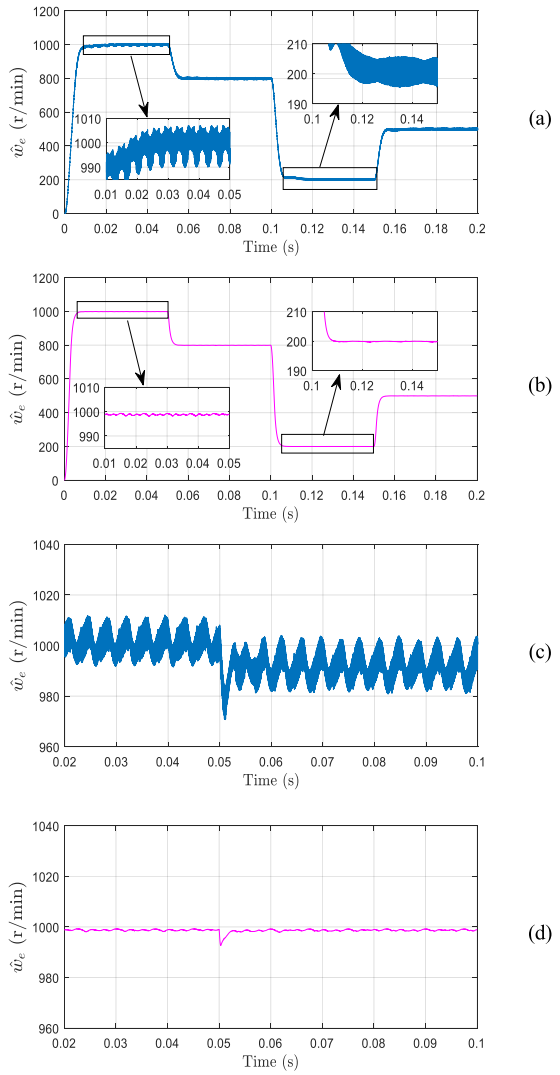

FIGURE 8. Various speed profiles and robustness analysis of two methods. (a) various speeds under the FSMO method. (b) various speeds under the IFSMO method. (c) sudden load under the FSMO method. (d) sudden load under the IFSMO method.

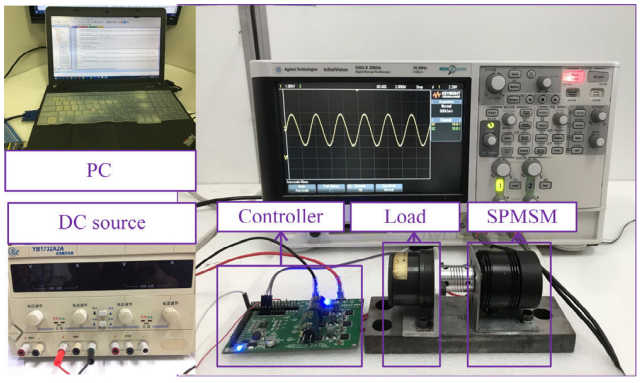

FIGURE 9. Experimental platform of the sensorless SPMSM system.

experimental platform is shown in Fig. 9, and the experimental parameters are consistent with the simulation parameters.

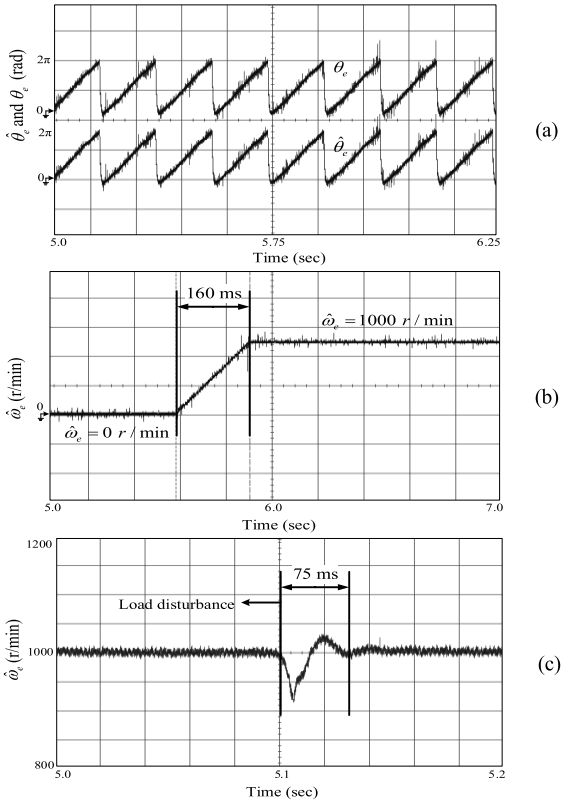

FIGURE 10. Experimental results under the FSMO method. (a) Rotor position. (b) Speed response. (c) sudden load.

Fig. 10 shows the experimental results of the motor running stably at 1000r/min after adopting the FSMO method. Fig. 10(a) displays the rotor position. Fig. 10(b) indicates the rotor speed waveform, and Fig. 10(c) depicts the speed waveform after suddenly adding the load on the SPMSM system when the rotor operates stably at 1000 r/min.

Fig. 11 displays the experimental results of the system under the IFSMO algorithm when the rotor is running at a steady speed of 1000 r/min. Fig. 11(a) shows the rotor position waveform, the rotor speed waveform is shown in Fig. 11(b), and Fig. 11(c) depicts the speed waveform after the load suddenly increases to the system when the rotor is running steadily at 1000 r/min.

By comparing the experimental results of Fig. 10 and Fig. 11, it can be observed that the start-up times of the motor system under the IFSMO method and FSMO method are 130 ms and 160 ms, respectively. Under the IFSMO and FSMO methods, the recovery time of the motor system subjected to the same disturbance is 50 ms and 75 ms, respectively. Moreover, the speed drop is smaller under the IFSMO method than that of the FSMO method. Consequently, we can draw the following conclusions: first, the SPMSM system based on the IFSMO method contains less high-frequency noise; second, the waveforms of the rotor speed and position are smoother, and the response time of the speed is shorter; third, the anti-disturbance capability of the system is further improved after using the IFSMO method.

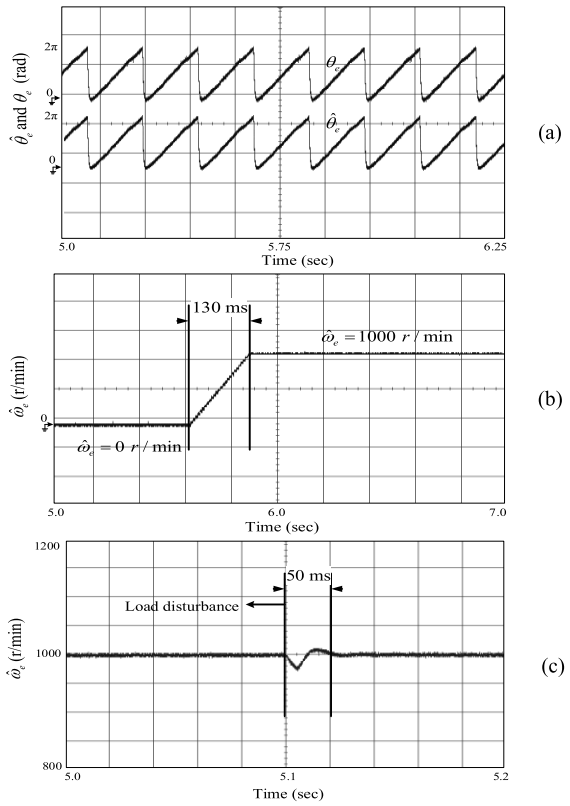

FIGURE 11. Experimental results under the IFSMO method. (a) Rotor position. (b) Speed response. (c) sudden load.

VI. CONCLUSION

This paper presents a speed- and position- sensorless strategy for the SPMSM system based upon the improved full-order sliding-mode observer. Firstly, a new switching function with a variable boundary layer instead of the sigmoid function is employed in the sliding-mode current observer. Secondly, a new sliding-mode function and the switching function are applied to the IFSMO, which improves the response performance and suppress the chattering. Thirdly, different from the conventional PLL method, the modified PLL technology with a signal suppressor is proposed to obtain the rotor position and speed. Moreover, the adaptive PI coefficients are used in PLL instead of fixed coefficients, which effectively enhances the performance of the SPMSM system. Finally, simulations and experiments are carried out to verify the effectiveness and superiority of the proposed method.

REFERENCES

[1] Z. Tang, X. Li, S. Dusmez, and B. Akin, "A new V/f-based sensorless MTPA control for IPMSM drives," *IEEE Trans. Power Electron.*, vol. 31, no. 6, pp. 4400–4415, Jun. 2016.

[2] P. D. C. Perera, F. Blaabjerg, J. K. Pedersen, and P. Thogersen, "A sensorless, stable V/f control method for permanent-magnet synchronous motor drives," *IEEE Trans. Ind. Appl.*, vol. 39, no. 3, pp. 783–791, May 2003.

[3] K. Li, G. Cheng, X. Sun, D. Zhao, and Z. Yang, "Direct torque and suspension force control for bearingless induction motors based on active disturbance rejection control scheme," *IEEE Access*, vol. 7, pp. 86989–87001, 2019.

[4] Z. Li, S. Zhou, Y. Xiao, and L. Wang, "Sensorless vector control of permanent magnet synchronous linear motor based on self-adaptive super-twisting sliding mode controller," *IEEE Access*, vol. 7, pp. 44998–45011, 2019.

[5] Y. Zhu, W. Gu, K. Lu, and Z. Wu, "Vector control of asymmetric dual three-phase PMSM in full modulation range," *IEEE Access*, vol. 8, pp. 104479–104493, 2020.

[6] F. Barati, R. Mcmahon, S. Shao, E. Abdi, and H. Oraee, "Generalized vector control for brushless doubly fed machines with nested-loop rotor," *IEEE Trans. Ind. Electron.*, vol. 60, no. 6, pp. 2477–2485, Jun. 2013.

[7] X. Fu and S. Li, "A novel neural network vector control technique for induction motor drive," *IEEE Trans. Energy Convers.*, vol. 30, no. 4, pp. 1428–1437, Dec. 2015.

[8] D. Liang, J. Li, R. Qu, and W. Kong, "Adaptive second-order sliding-mode observer for PMSM sensorless control considering VSI nonlinearity," *IEEE Trans. Power Electron.*, vol. 33, no. 10, pp. 8994–9004, Oct. 2018.

[9] J. Hu, J. Zou, F. Xu, Y. Li, and Y. Fu, "An improved PMSM rotor position sensor based on linear Hall sensors," *IEEE Trans. Magn.*, vol. 48, no. 11, pp. 3591–3594, Nov. 2012.

[10] C. M. Verrelli, S. Bifaretti, E. Carfagna, A. Lidozzi, L. Solero, F. Crescimbini, and M. D. Benedetto, "Speed sensor fault tolerant PMSM machines: From position-sensorless to sensorless control," *IEEE Trans. Ind. Appl.*, vol. 55, no. 4, pp. 3946–3954, Jul./Aug. 2019.

[11] W. Xu, S. Qu, L. Zhao, and H. Zhang, "An improved adaptive sliding mode observer for middle- and high-speed rotor tracking," *IEEE Trans. Power Electron.*, vol. 36, no. 1, pp. 1043–1053, Jan. 2021.

[12] J.-H. Im and R.-Y. Kim, "Improved saliency-based position sensorless control of interior permanent-magnet synchronous machines with single DC-link current sensor using current prediction method," *IEEE Trans. Ind. Electron.*, vol. 65, no. 7, pp. 5335–5343, Jul. 2018.

[13] S. Wang, K. Yang, and K. Chen, "An improved position-sensorless control method at low speed for PMSM based on high-frequency signal injection into a rotating reference frame," *IEEE Access*, vol. 7, pp. 86510–86521, 2019.

[14] I. Benlaloui, S. Drid, L. Chrifi-Alaoui, and M. Ouriagli, "Implementation of a new MRAS speed sensorless vector control of induction machine," *IEEE Trans. Energy Convers.*, vol. 30, no. 2, pp. 588–595, Jun. 2015.

[15] N. K. Quang, N. T. Hieu, and Q. P. Ha, "FPGA-based sensorless PMSM speed control using reduced-order extended Kalman filters," *IEEE Trans. Ind. Electron.*, vol. 61, no. 12, pp. 6574–6582, Dec. 2014.

[16] K. Zhao, T. Yin, C. Zhang, J. He, X. Li, Y. Chen, R. Zhou, and A. Leng, "Robust model-free nonsingular terminal sliding mode control for PMSM demagnetization fault," *IEEE Access*, vol. 7, pp. 15737–15748, 2019.

[17] Y. Chen, M. Li, Y.-W. Gao, and Z.-Y. Chen, "A sliding mode speed and position observer for a surface-mounted PMSM," *ISA Trans.*, vol. 87, pp. 17–27, Apr. 2019.

[18] S. Qu, X. Xia, and J. Zhang, "Dynamics of discrete-time sliding-mode-control uncertain systems with a disturbance compensator," *IEEE Trans. Ind. Electron.*, vol. 61, no. 7, pp. 3502–3510, Jul. 2014.

[19] Z. Qiao, T. Shi, Y. Wang, Y. Yan, C. Xia, and X. He, "New sliding-mode observer for position sensorless control of permanent-magnet synchronous motor," *IEEE Trans. Ind. Electron.*, vol. 60, no. 2, pp. 710–719, Feb. 2013.

[20] H. Kim, J. Son, and J. Lee, "A high-speed sliding-mode observer for the sensorless speed control of a PMSM," *IEEE Trans. Ind. Electron.*, vol. 58, no. 9, pp. 4069–4077, Sep. 2011.

[21] S. Lin and W. Zhang, "An adaptive sliding-mode observer with a tangent function-based PLL structure for position sensorless PMSM drives," *Int. J. Electr. Power Energy Syst.*, vol. 88, pp. 63–74, Jun. 2017.

[22] Z. Zhang, Y. Zhao, W. Qiao, and L. Qu, "A space-vector-modulated sensorless direct-torque control for direct-drive PMSG wind turbines," *IEEE Trans. Ind. Appl.*, vol. 50, no. 4, pp. 2331–2341, Jul./Aug. 2014.

[23] M. Zhou, Y. Feng, X. Yu, and F. Han, "Full-order terminal sliding-mode based energy saving control of induction motors," in *Proc. 43rd Annu. Conf. IEEE Ind. Electron. Soc. (IECON)*, Beijing, China, Oct. 2017, pp. 8208–8212.

[24] C. Yang, T. Ma, Z. Che, and L. Zhou, "An adaptive-gain sliding mode observer for sensorless control of permanent magnet linear synchronous motors," *IEEE Access*, vol. 6, pp. 3469–3478, 2018.

[25] L. Zhao, J. Huang, H. Liu, B. Li, and W. Kong, "Second-order sliding-mode observer with online parameter identification for sensorless induction motor drives," *IEEE Trans. Ind. Electron.*, vol. 61, no. 10, pp. 5280–5289, Oct. 2014.

[26] M. Defoort and M. Djemai, "A Lyapunov-based design of a modified super-twisting algorithm for the Heisenberg system," *IMA J. Math. Control Inf.*, vol. 30, no. 2, pp. 185–204, Jun. 2013.
[27] S. K. Kommuri, M. Defoort, H. R. Karimi, and K. C. Veluvolu, "A robust observer-based sensor fault-tolerant control for PMSM in electric vehicles," *IEEE Trans. Ind. Electron.*, vol. 63, no. 12, pp. 7671–7681, Dec. 2016.

WENJUN XU was born in Jingzhou, China. He received the M.Sc. degree in signal and information processing from Central China Normal University, Wuhan, China, in 2017, where he is currently pursuing the Ph.D. degree with the Department of Electronics and Information Engineering. His research interests include electric machines and drives, power electronics, and sliding mode control.

SHAOCHENG QU (Senior Member, IEEE) was born in Hubei, China. He received the B.Sc. degree in process control and instrument from the Wuhan University of Chemical and Technology, Wuhan, China, in 1994, the M.Sc. degree in control engineering from the Naval University of Engineering, Wuhan, in 2000, and the Ph.D. degree in control theory and control engineering from the Huazhong University of Science and Technology, Wuhan, China, in 2004.

He is currently a Full Professor with the Department of Electronics and Information Engineering, College of Physical Science and Technology, Central China Normal University, Wuhan. His research interests include sliding mode control, control theory and applications, intelligent information processing and control, embedded systems, and the Internet of Things (IoT) system applications. He has published more than 80 articles on these topics and published a monograph on SMC theory and applications, in Chinese. He also provides consultancy to various industries.

JINGHONG ZHAO was born in 1975. He received the Ph.D. degree in electrical engineering from the Naval University of Engineering, Wuhan, China, in 2011. He is currently a Professor with the School of Electricity Engineering, Naval University of Engineering. He has authored or coauthored more than 50 articles. His current research interests include power electronics, electric machine design, and its control.

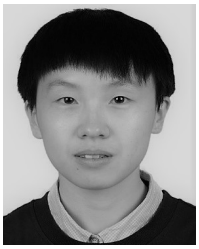

HONGRUI ZHANG was born in Xiaoyi, China. She received the master's degree in electronics and communication engineering from Northwest Normal University, Lanzhou, China, in 2018. She is currently pursuing the Ph.D. degree with Central China Normal University, Wuhan, China. Her main research interests include image processing and electronics.

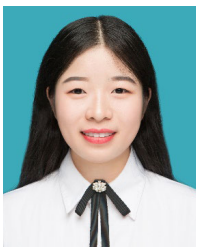

XIAONA DU received the master's degree in mathematics from China Three Gorges University, Yichang, China, in 2020. She is currently pursuing the Ph.D. degree with Central China Normal University, Wuhan, China. Her research interests include complex dynamical networks, sampled data, and multi-agent systems.